Microindentation and XPS Characterization of ACD Ni-P

L. Magagnin,[1] M. Ghilardi,[1] F. Pagano,[1] L. Lombardi[2],
V. Sirtori[2] and P.L. Cavallotti[1]
[1]Dip. Chimica, Materiali e Ingegneria Chimica, Politecnico di Milano, Milano, Italy
[2] Celestica, Vimercate, Italy

Nanocrystallization and strain recovery of ACD Ni-P during microindentation creep tests under constant load are investigated. Stress-strain curves with dwell times 1 - 60 s are obtained and loads in the range 1-100 mN are applied for 60 s during creep tests. Under constant load, ACD medium-high phosphorus Ni-P can show a progressive recovery of the deformation. This depends on the local indentation point. When a structure transition is induced by heat treatment from amorphous to crystalline Ni-P, the penetration depth recovery during creep is decreased. Evolution and rearrangement of the local microstructure are suggested to explain the strain recovery under constant load. Ni-P films are characterized by XPS angle resolved technique before and after sputtering. The energy of the Ni maximum peak in the valence band of Ni-P film corresponds to that of metallic nickel, with binding energy 0.75 eV. No detectable difference was found between the binding energy of nickel in the pure metallic state and in the Ni-P coating, suggesting a similar chemical state for nickel in both conditions.

For more information, contact:
P.L. Cavallotti
Dip. Chimica, Materiali e Ingegneria Chimica “Giulio Natta”
Politecnico di Milano
Via Mancinelli,7 - 20131 Milano, Italy
Phone: +39-02-23993149
Fax: +39-02-23993180
E-mail: pietro.cavallotti@polimi.it

Introduction

Indentation is an accurate technique for the mechanical characterization of thin films. Simultaneous recording of load and depth permits calculation of mechanical quantities, such as hardness and a comprehensive elastic modulus, with high accuracy and repeatability. A further depth increase is observed when the load is maintained constant at its maximum value.[1,2] To date, the creep behavior of materials during indentation and particularly the effect of negative creep observed for some materials was not investigated in details.[3]

The phenomenology of negative creep, i.e. contractive specimen length change under tensile creep test conditions, is known for nickel superalloys at high temperatures. The measured negative creep results from the superposition of two opposite processes. These are the common plastic creep and the simultaneous volume contraction as a consequence of a thermally unstable phase microstructure.[3] Using the field ion microscope and the atom probe on nickel-base superalloys after creep test, an atomic arrangement of the metal surface was observed in correspondence to a negative creep behavior.[4] Nimonic 80A shows an increasing stress with increasing duration of constant-strain stress relaxation tests at 550 °C. This is contrary to the normally observed stress relaxation behavior and was termed negative creep. Negative creep was related to the contraction of the material during test.[5]

Recovery of indentation was observed during indentation creep on MgO crystals. Analysis of the kinetics suggests that recovery occurs by local reorganization, and volume and surface diffusion processes above a threshold value of the indentation pressure gradient.[6]

In this work, the mechanical behavior of autocatalytic Ni-P deposits under constant load during indentation test at room temperature is investigated. Autocatalytic Ni-P deposits are metastable phases in which phosphorus is occluded in a nickel matrix. Low phosphorus deposits (1-3 %wt P) are crystalline, while medium phosphorus deposits (5-8 %wt P) tend to be semi-amorphous. High phosphorus deposits (more than 10 %wt P) are recognized as metallic glasses. According to the phosphorus content, Ni-P upon annealing can transform into Ni + Ni_3P phases or into a nickel matrix plus complex morphology compounds.

In this work, the mechanical behavior of autocatalytic Ni-P deposits was investigated after annealing and crystallization. Ni-P deposits are characterized by XPS before and after sputtering with argon ions. Displacement of nickel atoms due to argon ion implantation is taken into account. The formation of metallic nickel in the first layer is detected after sputtering by X-ray diffractometry at low glancing angle. No detectable difference was found between the binding energy of nickel in the metallic state and in the Ni-P coating, showing a similar chemical state for nickel in both conditions.

Experimental

The Ni-P film, about 20 µm thick, was obtained by Autocatalytic Chemical Deposition ACD on titanium. ACD was carried out from an electrolyte of nickel acetate $Ni(CH_3CO_2)_2\ 4H_2O$ 0.12 M, sodium hypophosphite NaH_2PO_2 0.32 M, lactic acid $CH_3CH(OH)CO_2H$ 0.5 M at pH = 4.7, T = 85 °C. The Ni-P coating was rinsed with deionised DI water and dried with nitrogen. Ni-P

deposits were removed from the substrate and embedded between two steel sheets in epoxy resins. The embedded sample's cross-sections were polished with emery paper.
Scanning Electron Microscopy (SEM) experiments were performed with a Cambridge Stereoscan 360 with 10^{-5} – 10^{-7} Torr vacuum. X-ray diffraction (XRD) experiments with a Bragg-Brentano configuration were performed in a Philips PW 1830 instrument, with a goniometer Philips PW 3020 and a control unit Philips PW 3710 (Cu K_α radiation with wavelength 1.5406 Å, scan rate 1 degree per minute). Microhardness was measured on the cross-section by depth-sensing technique with a FISCHERSCOPE® H100 computer-controlled system with Vickers indenter. Load was applied in 10 sec, held for 60 sec and then unloaded in 10 sec.
XPS measures were carried out with a PHI 5600ci spectrometer, equipped with a monochromated Al Kα X-ray source (Kα = 1486.6 eV) and a spherical capacitor analyser (SCA). The instrument was calibrated periodically by means of Ag $3d_{5/2}$ (368.3 eV), Au $4f_{7/2}$ (84 eV) and Cu $2p_{3/2}$ (932.7 eV) standards. XPS photoemission peaks of Ni $2p_{3/2}$, P 2p and Ar 2p were used to calculate the relative atomic concentrations. Ar^+ bombardment was employed to sputter about 30 nm in depth. Sputtered area was 15 mm x 18 mm, with primary beam diameter 250 μm, energy was 2 or 5 keV and current 1.5 or 6 μA, respectively. The correspondent ion fluxes were 1.7 10^9 and 6.8 10^9 ions/μm^2 s. The ion gun was set at 45° with respect to the specimen axis. The sputtering rate was calibrated by ion etching a tantalum specimen covered with a Ta_2O_5 layer of known thickness. The etching rate was 0.05 nm/min for 1.5 μA and 0.2 nm/min for 6 μA, corresponding approximately to 0.125 nm/min and 0.5 nm/min in the case of nickel specimens. The total sputtering time was about 4 and 1 hour, respectively. In order to obtain the depth distribution of phosphorus, the angle resolved technique was employed with take off angle (with respect to the sample surface) 5°, 20°, 45°.

Results and discussion
Autocatalytic Ni-P films were characterized by a P content of 10 %wt and the film structure was amorphous. Fig. 1 shows the XRD patterns of the Ni-P films before and after annealing at different temperature. With annealing at 150 °C for 1 hr, it was observed a first reorganization of the amorphous structure. After heat treatment at 400 °C for 1 hr, the amorphous structure was transformed in the Ni + Ni_3P structure. The amorphous-crystalline transformation was completed after annealing at 600 °C for 24 hr.

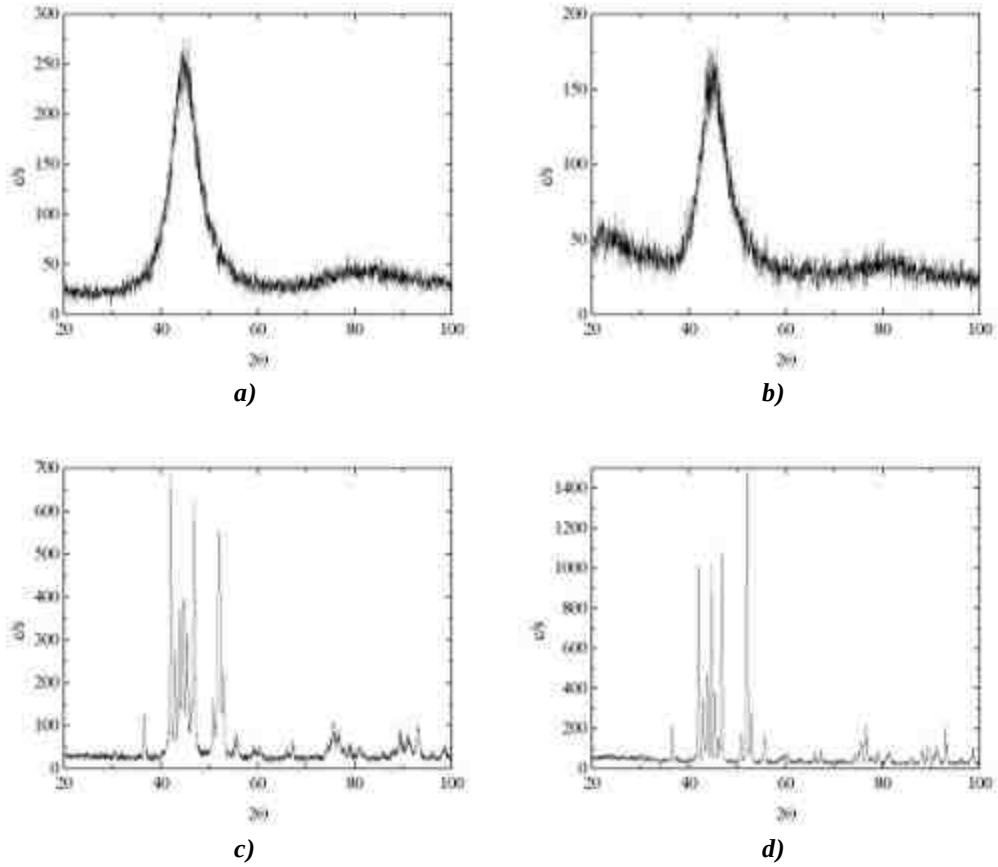

Fig. 1 *- XRD patterns of the Ni-P films a) before annealing, b) after annealing at 150 °C for 1 hr, c) after annealing at 400 °C for 1 hr, and d) after annealing at 600 °C for 24 hr.*

Table 1-3 reports the quantities obtained in the indentation tests for Ni-P films before and after annealing. For different loads, creep percentage, elastic modulus Y, Vickers Hardness HV, maximum penetration depth Hmax, and the elastic to total work ratio are reported.

Table 1 *– Indentation results on Ni-P film without annealing.*

Load	**Creep** (%)	**Y** (GPa)	**HV**	**Hmax** (μm)	**We/Wtot** (%)
5	-23.4	151	1807	0.115	52
10	-12.3	130	1081	0.189	43
50	-5.1	120	736	0.538	36
100	-3.7	104	625	0.866	37

Table 2 *– Indentation results on Ni-P film after annealing at 150 °C for 1 hr.*

Load	Creep (%)	Y (GPa)	HV	Hmax (μm)	We/Wtot (%)
5	-5.5	131	1140	0.107	48
10	-11.9	143	1179	0.173	42
50	-3.4	119	715	0.534	36
100	-2.8	119	693	0.802	36

Table 3 *– Indentation results on Ni-P film after annealing at 400 °C for 1 hr.*

Load	Creep (%)	Y (GPa)	HV	Hmax (μm)	We/Wtot (%)
5	-1.9	161	1779	0.085	68
10	-1.5	148	1428	0.144	58
50	-1.1	152	1075	0,429	45
100	-0.5	136	951	0.689	45

Vickers hardness increases with decreasing applied load. Divergences at low loads are documented for many materials and can be related to the contribution of surface energy, dislocation mobility or indentation size effect.[7,8,9] After annealing and crystallization, Vickers hardness increases due to the separation of Ni_3P in the prime Ni matrix. Also elastic modulus slightly increases with annealing temperature and time.
Contrary to what expected, creep values were negative and less negative with increasing load and temperature annealing. Negative creep values were related to the rising of the indenter during the constant load creep tests. Under constant load, ACD medium-high phosphorus Ni-P can show a progressive recovery of the deformation. This depends on the local indentation point. When a structure transition is induced by heat treatment from amorphous to crystalline Ni-P, the penetration depth recovery during creep is decreased. Evolution and rearrangement of the local microstructure are suggested to explain the strain recovery under constant load. Negative creep was not associated with any gradient in the composition of the Ni-P film, as shown in the following XPS analyses.

The mechanical behavior of Ni-P under constant load and the observed strain recovery are in agreement with the surface modification of very flat Ni-P films after ion beam treatment.[10] The ion bombardment was effected to decrease the surface stress, but induced formation of circular localized structures at the surface with evident pile up at the edge was observed. Fig. 2 and 3 show examples of Ni-P surfaces after ion bombardment. Due to oscillating deposition of nickel and phosphorus, ACD Ni shows an atomically stratified structure. The wave-shape formations are explained through a local rearrangement of Ni-P occurring with periodic variations of composition. This gives surface ridges of 2-3 nm height.

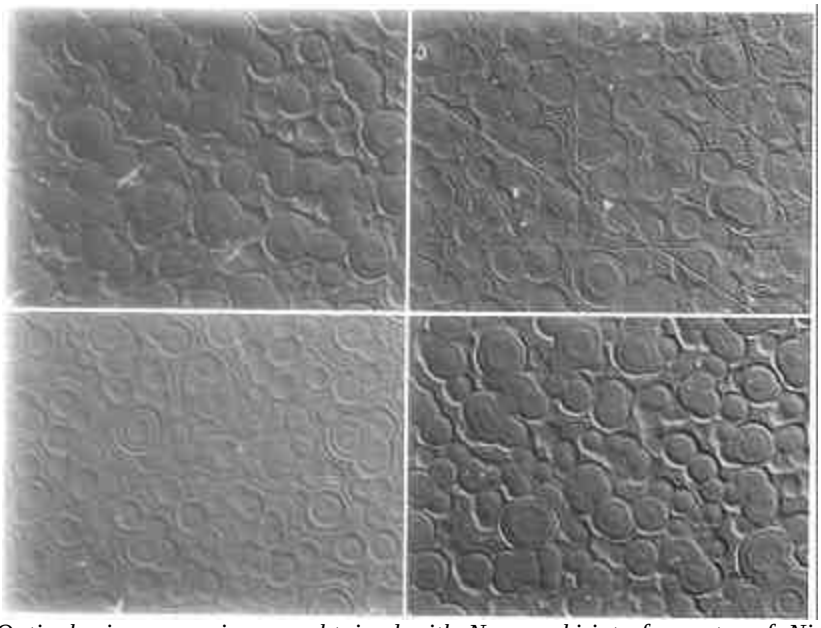

Fig. 2 *– Optical microscope images obtained with Normarski interferometer of Ni-P surface after ion beam bombardment.*

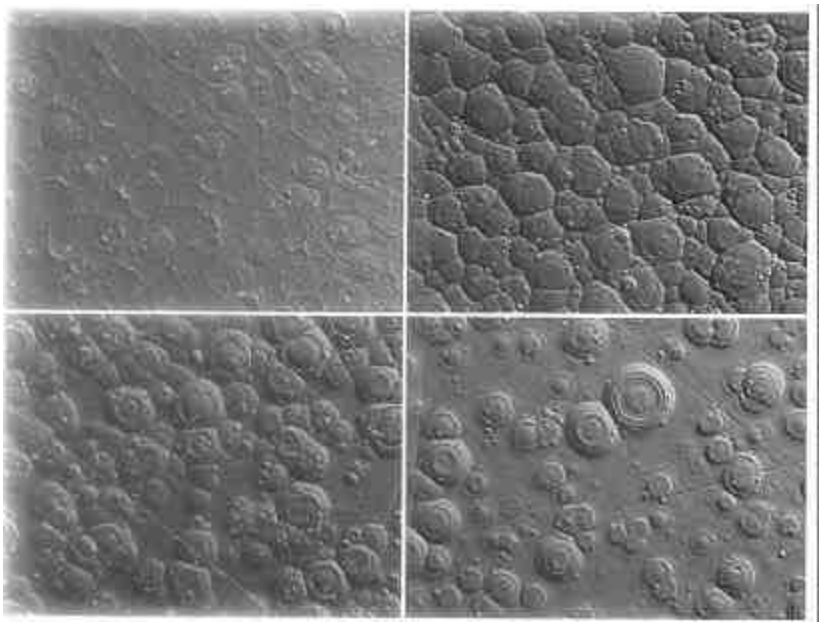

Fig. 3 *– Optical microscope images obtained with Normarski interferometer of Ni-P surface after ion beam bombardment.*

Piles up of the circular structures recall the pile up effect during indentation, likely due to a similar evolution and reorganization of the local surface structure under localized stress. When pile up edges run into other edges, a well define surface is formed and maintained. Further investigations are required to assess the evolution of the crystallographic structure.

Table 4 gives nickel and phosphorus atomic percentage concentration at different take off angles. Ni and P atomic percentage concentration are corrected according to the model described in Ref. 11, to take into account argon implantation during sputtering. Corrected XPS data are in good agreement with EDS/SEM data and shows that the composition of the Ni-P film is homogeneous with depth.

Table 4 *– Ni and P atomic percentage compositions obtained at different take off angle and sputtering energy for a Ni-P film.*

Sputter energy (keV)	**Take off angle**	**Ni** (%at)	**P** (%at)
2	5°	89.33	10.67
2	20°	90.96	9.04
2	45°	91.84	8.16
5	5°	90.80	9.20
5	20°	89.91	10.19
5	45°	91.11	8.89

Comparing XPS spectra in the valence band region of pure Ni and Ni_2P as reference, with Ni-P of similar content implanted with argon ions, Ni-P and pure nickel showed a very similar behavior. The maximum peak is about 0.74 eV negative with respect to the Fermi energy, whilst in the case of Ni_2P the maximum is at 1.1 eV. The only difference observed between pure Ni and Ni-P regards the number of states for the 4d valence band at the Fermi level, decreasing from 0.39 for pure Ni to 0.34 for Ni-P.

A low-phosphorus Ni-P film on copper-sputtered silicon was characterised by XPS analysis before and after annealing at 600 °C for 2 hr. Table 5 and 6 report the atomic concentrations at the surface and after sputtering.
Before annealing, P content was about 5 % at the surface and about 3 % at 150 Å depth. After heat treatment, it was about 7 % at the surface and 4 % at 150-300 Å depth. Annealing slightly increased the oxygen content at the surface from 31.35 % to 39.04 %. XPS spectrum at the surface for Ni $2p_{3/2}$ photoemission peak in fig. 4 shows two contributions at 852.3 eV and 856.3 eV related to pure nickel and to $Ni(OH)_2/NiPO_x$ species respectively. Presence of PO_x species was confirmed by P $2p_{3/2}$ spectrum, in fig. 5, which can be decomposed in two peaks at 129.4 eV and 132.9 eV related to elemental P and PO_x species respectively. After sputtering, only pure nickel and phosphorus were detected, as shown in the Ni and P photoemission spectra in fig. 6.
After annealing, Ni $2p_{3/2}$ photoemission peak at the surface, shown in fig. 7, was composed of two contributions at 852.7 eV and 856.5 eV related to pure nickel and $Ni(OH)_2/NiPO_x$ species respectively. P $2p_{3/2}$ photoemission peak, shown in fig. 8, was mainly composed by PO_x species contribution at 133.5 eV. After sputtering, only pure nickel was detected and phosphorus peak showed a smaller FWHM than before sputtering.

Table 5 *– XPS atomic concentrations on Ni-P before annealing.*

C 1s	N 1s	O 1s	Si 2p	P 2p	Ni 2p	Depth
52.67	0.81	31.35	1.56	5.24	8.37	surface
0	0	0	0	3.14	96.86	150 Å

Table 6 *– XPS atomic concentrations on Ni-P after annealing at 600 °C for 2 hr.*

C 1s	N 1s	O 1s	Si 2p	P 2p	Ni 2p	Depth
42.79	-	39.04	3.51	7.46	7.21	surface
0	-	1.30	0	3.78	94.92	150 Å
0	-	0	0	4.00	96.00	300 Å

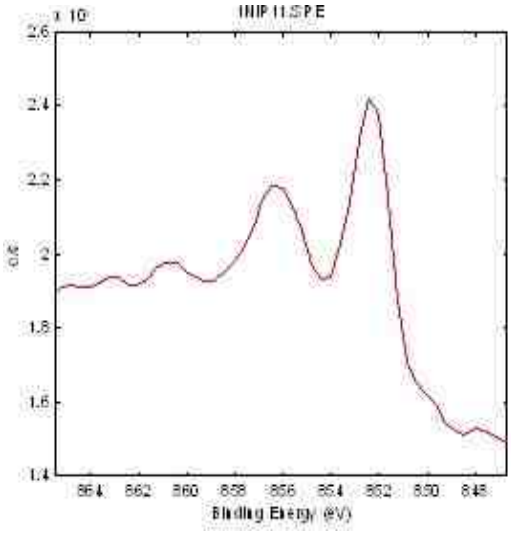

Fig. 4 *– Ni $2p_{3/2}$ photoemission peak for Ni-P at the surface before annealing.*

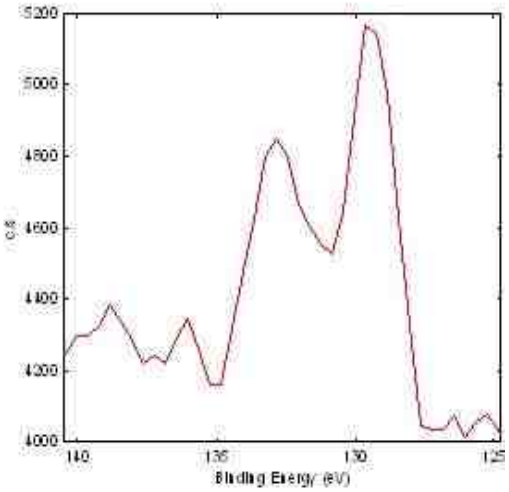

Fig. 5 *– P $2p_{3/2}$ photoemission peak for Ni-P at the surface before annealing.*

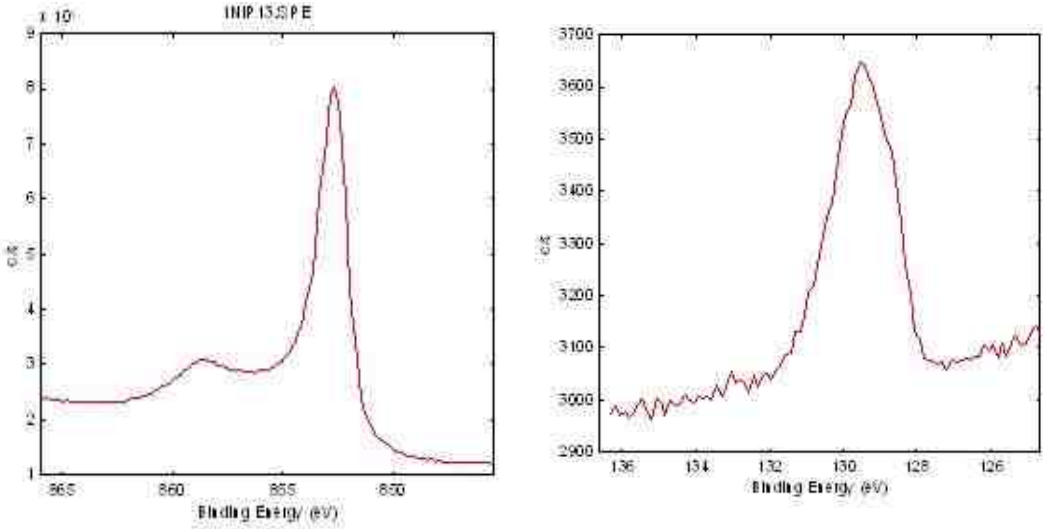

Fig. 6 *– Ni $2p_{3/2}$ (left) and P $2p_{3/2}$ (right) photoemission peaks for Ni-P before annealing and after sputtering.*

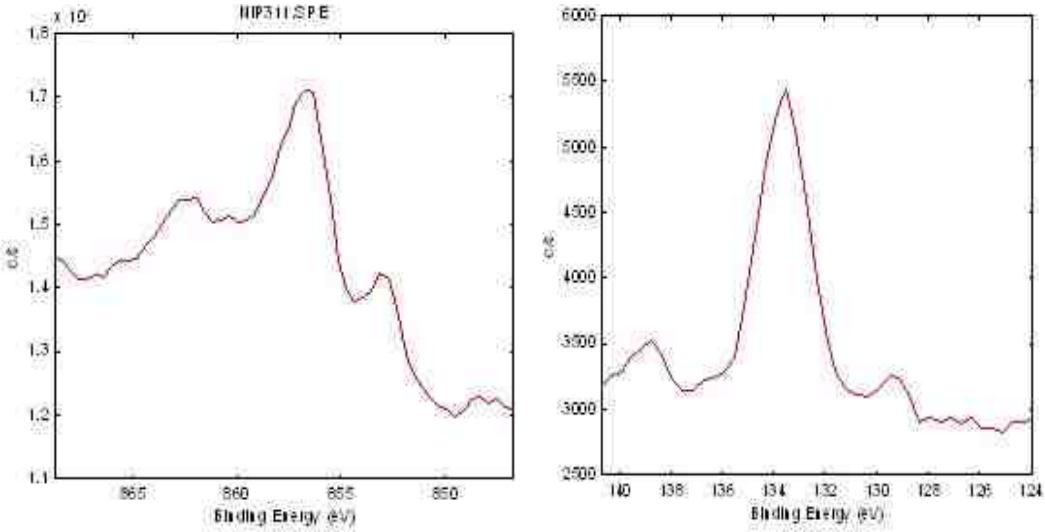

Fig. 7 *– Ni $2p_{3/2}$ photoemission peak for Ni-P at the surface after annealing at 600 °C for 2 hr.*

Fig. 8 *– P $2p_{3/2}$ photoemission peak for Ni-P at the surface after annealing at 600 °C for 2 hr.*

Conclusions

The mechanical behavior of autocatalytic Ni-P deposits under constant load during indentation test at room temperature was investigated. Vickers hardness increases with decreasing applied load and after annealing. Contrary to what expected, creep values could be negative with increasing load and less negative with temperature annealing. Under constant load, ACD Ni-P was characterized by a progressive recovery of the deformation. When a structure transition is induced by heat treatment from amorphous to crystalline Ni-P, the penetration depth recovery

during creep is decreased. Evolution and rearrangement of the local microstructure are in agreement with surface modification after ion beam bombardment and suggested to explain the strain recovery under constant load.
Comparing XPS spectra in the valence band region, Ni-P and pure nickel showed a very similar behavior. Presence of $Ni(OH)_2/NiPO_x$ species at the surface was detected in the photoemission peak spectra for nickel and phosphorus.

Acknowledgement
Dr. Citterio and coworkers of Laboratorio Astrofisico di Merate are gratefully acknowledged for the images obtained with the Normarski interferometer optical microscope.

References
1. F. Frohlich, P. Grau, W. Grellmann, *Phys. Stat. Sol. A*, **42**, 79 (1977).
2. T. Chudoba, F. Richter, *Surface and Coating Technology*, **148**, 191 (2001).
3. B. Reppich, *Z. Metallkd.*, **85**, 28 (1994).
4. D.G. Ren, *Journal of Materials Processing Technology*, **73**, 74 (1998).
5. E. Metcalfe, B. Nath, A. Wickens, *Materials Science and Engineering*, **67**, 157 (1984).
6. K. Sangwal, P. Gorostiza, F. Sanz, *Surface Science*, **446**, 314 (2000).
7. H.-J. Weiss, *Phys. Stat. Sol. (a)*, **99,** 491 (1987).
8. R.W. Armstrong, A.W. Ruff, H. Shin, *Materials Science and Engineering*, **A209**, 91 (1996).
9. J.R. Tuck, A.M. Korsunsky, R.I. Davidson, S.J. Bull, D.M. Elliott, *Surf. Coat. Technol.*, **127**, 1 (2000).
10. P.L. Cavallotti, *Galvanotecnica e nuove finiture*, **3**, 142 (1997).
11. V. Sirtori, L. Lombardi, P.L. Cavallotti, L. Magagnin, *Applied Surface Science*, in press.